PERGAMON

Continental Shelf Research 18 (1998) 541–559

CONTINENTAL SHELF RESEARCH

Assimilation of Doppler radar current data into numerical ocean models

James K. Lewis[a,*], Igor Shulman[b], Alan F. Blumberg[c]

[a]*Ocean Physics Research and Development, 207 S. Seashore Drive, Long Beach, MS 39560, USA*
[b]*Center for Ocean and Atmospheric Modeling, The University of Southern Mississippi, Stennis Space Center, MS 39529, USA*
[c]*HydroQual, Inc., 1 Lethbridge Plaza, Mahwah, NJ 07430, USA*

Received 15 May 1997; accepted 22 December 1997

Abstract

A technique is presented for the assimilation of ocean surface currents determined from Doppler radar systems into numerical ocean models. An approach is taken in which the Doppler radar current data act as if there were an additional layer of water overlying the ocean surface. A pseudo-shearing stress resulting from the difference between the model-predicted velocity and the Doppler radar velocity is added to that of the wind in order to force a model.

Test applications are presented for an ocean model of the Monterey Bay, California, region. Comparisons are made between optimized and non-optimized assimilation techniques based on the shearing stress approach. The optimized assimilation scheme provides the minimum additional shearing stress while achieving a significant nudging of the model surface currents toward the basic characteristics of the observed field of Doppler radar currents. Analyses indicate that the model surface currents take on the general pattern of the Doppler radar currents but not always the magnitude. The radar currents are shown to have significant divergences and unrealistic spatial variations of divergence. Characteristics of this sort for oppler data suggest additional processing for such observations.

Key words: Data assimilation; Ocean modeling; Doppler current data.

1. Introduction

High frequency Doppler radar systems have been used over the last 20 years to estimate surface currents over ocean regions, usually coastal areas. The Doppler systems have developed to the stage that their costs and processing times allow for

* Corresponding author.

0278–4343/98/$19.00
PII S0278–4343(98)00006–5

a near-real-time determination of a grid of surface currents every 20–30 min for most regions of interest. Such systems provide a valuable set of information which can be utilized in numerical ocean models.

A recent study using Doppler radar systems in Monterey Bay, California, area has provided comparisons between such radar surface current data, acoustic Doppler current profiler (ADCP) data ($\sim$ 9 m below the surface) and drifter data (Paduan and Rosenfeld, 1996). The HF Doppler Radar observations represented an average over a region about 4 km^2 and about 1–2 m deep. The comparisons with the more pointwise ADCP and drifter data showed significant differences. If the ADCP and drifter data were completely error-free, the comparisons would imply that the HF Doppler radar current data were accurate 50% of the time to within 7 cm/s. Seeing that the currents in Monterey Bay are of the order of 10–30 cm/s, these results would imply that the accuracy of the Doppler data can be rather poor at times. Intercomparisons of Doppler systems within Monterey Bay indicate that the differences between the currents sensed in the same grid area at the same time by two different HF systems can be fairly large with respect to the magnitude of the current, of the order of 10–15 cm/s (J. Paduan, personal communication). Thus, the current information provided by HF Doppler radar systems may be useful in terms of trends, the pattern of currents, and general magnitudes, but care must be taken in the assimilation of such data into numerical models.

One strategy of assimilating Doppler current observations into an ocean model is based on the application of a shearing stress over the surface layer of the model. This surface shearing stress would include not only the wind stress but also a pseudo-stress resulting from the difference between the model-predicted velocity and the velocity observed by a HF Doppler system. This approach is in effect a nudging technique, with the net acceleration being only partly a result of the observed HF Doppler current data. However, if the differences between the model and observed currents are great enough, the pseudo-shearing stress may become considerable. In this work, we develop an optimized approach to the assimilation of HF Doppler current data. In the application of the optimized assimilation scheme, it is shown that the additional shearing stress can be minimized while achieving a significant nudging of the model results toward the basic characteristics of the observed field of Doppler currents. The results of our work indicate that Doppler current data could be further processed to conform to the tenants of near non-divergence and no flow through a shoreline.

In Section 2 we outline our approach in developing an optimized assimilation scheme for HF Doppler current observations. The ocean model for the Monterey Bay coastal region is presented in Section 3 along with boundary forcing and formulations. In Section 4 we present the results of a number of test simulations for assimilating Doppler current information into the Monterey Bay regional model. Section 5 presents a discussion of the results of our study.

2. Approach

Our approach is to formulate an assimilation technique based on a shearing stress acting on the ocean surface. This shearing stress will be a result of the differences

between the model and Doppler current observations and will be added to any stress due to wind forcing. The net surface stress is then used by the model in the typical fashion of surface wind stress forcing. For the time being, we shall neglect wind stress.

We can formulate a shearing stress that nudges the model solution toward the Doppler current observations by parameterizing a shearing stress vector τ_s on the ocean surface in a non-linear fashion following standard conventions:

$$\tau_s = \rho C_D(\mathbf{U} - \mathbf{u})|\mathbf{U} - \mathbf{u}|, \tag{1}$$

where ρ is the water density, C_D is a drag coefficient (order of 10^{-3}), $\mathbf{U}$ is the observed Doppler radar velocity, and $\mathbf{u}$ is the model-predicted velocity. In effect, we are allowing the HF Doppler data to act as if there were an additional layer of water overlying the ocean surface, and Eq. (1) represents the shearing stress between the ocean surface and this pseudo-layer of water.

The drag coefficient C_D can be considered as a nudging parameter. But the high level of uncertainties in the accuracy of the Doppler radar currents makes the problem of estimating C_D rather complicated. Suppose the value of C_D is arbitrarily set to a given value. Then the integral

$$\int_A \tau_s * (\mathbf{U} - \mathbf{u})\, dA$$

where A is the ocean surface, represents the work performed by the shearing stress relative to the differences between the model-predicted and observed currents. We will define another shearing stress τ based on the following optimization problem:

$$\min_{\tau}\left[J(\tau) = \int_A (\tau * \tau)/\rho C_D\, dA\right]$$

constrained by the relationship

$$\int_A \tau * (\mathbf{U} - \mathbf{u})\, dA = \int_A \tau_s * (\mathbf{U} - \mathbf{u})\, dA,$$

where τ_s is given by Eq. (1). Physically, the above problem means that we will chose the minimal shearing stress which performs the same work over the ocean surface as the stress given in Eq. (1). This will lead to a gentle nudging of the observed Doppler currents in the model dynamics.

The solution to the above problem has the form

$$\tau = \lambda \rho C_D(\mathbf{U} - \mathbf{u}), \tag{2}$$

where the Lagrange multiplier is given by

$$\lambda = \int_A \tau_s(\mathbf{U} - \mathbf{u})\, dA \Big/ \int_A \rho C_D|\mathbf{U} - \mathbf{u}|^2\, dA. \tag{3}$$

Substituting Eq. (3) into Eq. (2) gives an expression that can be used to calculate the shearing stress at an i,j model grid cell in terms of the grid cell Doppler observation $\mathbf{U}_{i,j}$ and the grid cell model-predicted velocity $\mathbf{u}_{i,j}$:

$$\tau_{i,j} = (\mathbf{U}_{i,j} - \mathbf{u}_{i,j})\rho C_D \int_A (\mathbf{U} - \mathbf{u})^2 |\mathbf{U} - \mathbf{u}| \, dA \Big/ \int_A |\mathbf{U} - \mathbf{u}|^2 \, dA.$$

3. Model formulation

3.1. The numerical model

To test assimilation schemes, a numerical ocean model was constructed for the Monterey Bay, California, region (Fig. 1). The hydrodynamic model used in this work is an adaptation of the model of Blumberg and Mellor (1987). The model is based on

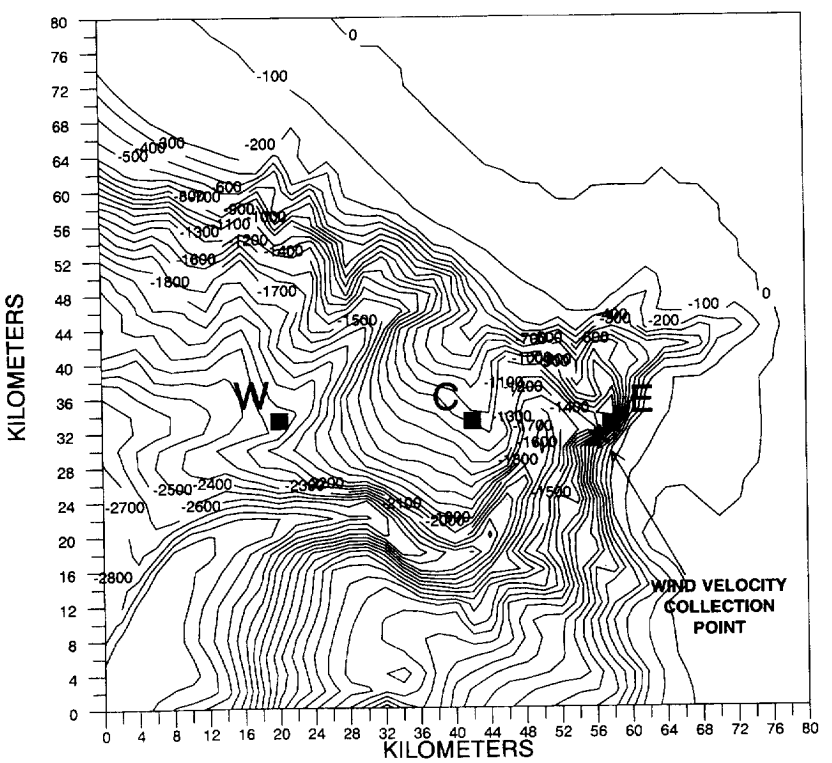

Fig. 1. Domain and bathymetry of the ocean model. Depth contours are in meters at 100 m intervals. The asterisk near the mouth of the Monterey Bay represents the location where wind velocity data were collected. Stations W (west), C (center), and E (east) are locations at which rms differences between model surface currents and Doppler currents are considered.

the primitive equations for momentum, salt, and heat. Sub-grid scale turbulence is specified using the schemes of Mellor and Yamada (1982) in the vertical and Smagorinsky (1963) in the horizontal. For additional information on the model, the reader is referred to Blumberg and Mellor (1987).

This particular version of the Blumberg–Mellor model uses a semi-implicit solution scheme for solving for the surface height field (Casulli and Cheng, 1992). The original Casulli and Cheng implicit solver uses the water velocities at a previous time level for the Coriolis term. For flows with inertial oscillations, such a formulation will require a very small time step to overcome numerical stability considerations. The implicit solution scheme used in this study uses both the past and future velocities to determine the Coriolis effect, iterating to obtain a solution at each time step.

Another modification of the original Blumberg–Mellor model is the use of a hybrid z-level coordinate system in the vertical. The original model uses a bottom-following sigma-coordinate grid in the vertical. However, there are often problems with a sigma-coordinate system when going over relatively steep bathymetry and using realistic temperature and salinity (T–S) structure. Since we wish to model the shallow shelf region out to the shelf break and then over the shelf slope, the hybrid z-level vertical coordinate system discussed by Lewis et al. (1994) was used to eliminate any problems that could arise from the application of sigma-coordinates. In this scheme, water velocities are calculated using the momentum equations in a vertically averaged mode using actual bathymetry. These velocities are saved, and the model is then executed for the same time step in a z-level mode to calculate the three-dimensional field of currents using a step-wise approximation to the bathymetry. The transports calculated using the step-wise approximation to the bathymetry are then adjusted (barotropically) to match the transports calculated in the vertically average mode. Since the latter mode uses actual bathymetry, this adjustment allows longwaves to propagate at appropriate speeds across the domain of the model.

The model has a rectangular grid with a 2 km × 2 km horizontal resolution. The vertical structure of the model is shown in Table 1. The horizontal and vertical resolutions are appropriate for the HF Doppler current data that are to be assimilated into the model (Paduan and Rosenfeld, 1996). Existing summer-time observations were used to initialize the model with a horizontally constant vertical profile of temperature and salinity (Fig. 2). The importance of using a good approximation of the water column stratification should be noted. The stratification at the bottom of the surface mixed layer inhibits the downward flux of those stresses induced by differences between the model and Doppler radar currents. Without such stratification, the assimilation technique could result in a continued downward flux of energy throughout the water column, and this could impact the ability of the model to provide reasonable subsurface predictions of currents.

3.2. *Surface forcing: Doppler current data and winds*

The HF Doppler radar observations used in this work were collected in the Monterey Bay area, and details of the complete data set are discussed by Paduan and Rosenfeld (1996). All Doppler data collected during August 1994 were sampled at two

Table 1
Characteristics (m) for the levels in the model for Monterey Bay

Layer	Top of layer	Bottom of layer	Layer thickness
1	0	2	2
2	2	3	1
3	3	4	1
4	4	6	2
5	6	10	4
6	10	15	5
7	15	20	5
8	20	30	10
9	30	40	10
10	40	60	20
11	60	80	20
12	80	100	20
13	100	150	50
14	150	200	50
15	200	400	200
16	400	1000	600
17	1000	1500	500
18	1500	2000	500
19	2000	2500	500
20	2500	3300	800

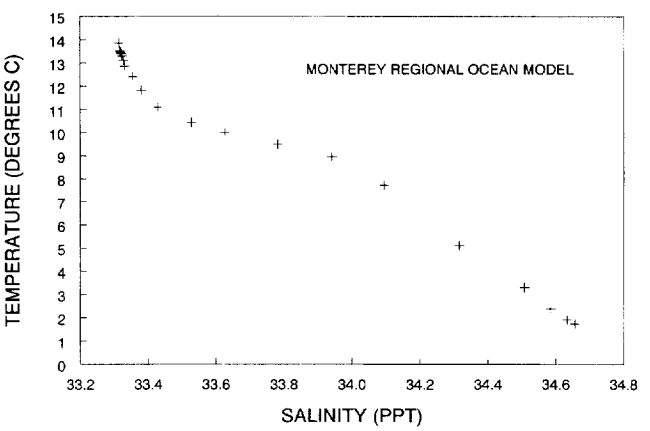

Fig. 2. Temperature–salinity used for initializing the temperature and salinity for the levels in the model. The + 's indicated the T–S value used for each level, starting with the surface level (upper left) to the bottom level (lower right).

hour intervals, and velocities were linearly interpolated to obtain Doppler currents at the time step of the ocean model. Observations from station E (Fig. 1) are shown in Fig. 3. These currents represent 30 min averages over about a 4 km^2 region. Tidal oscillations are evident in the velocity data, and there is a distinct net southward

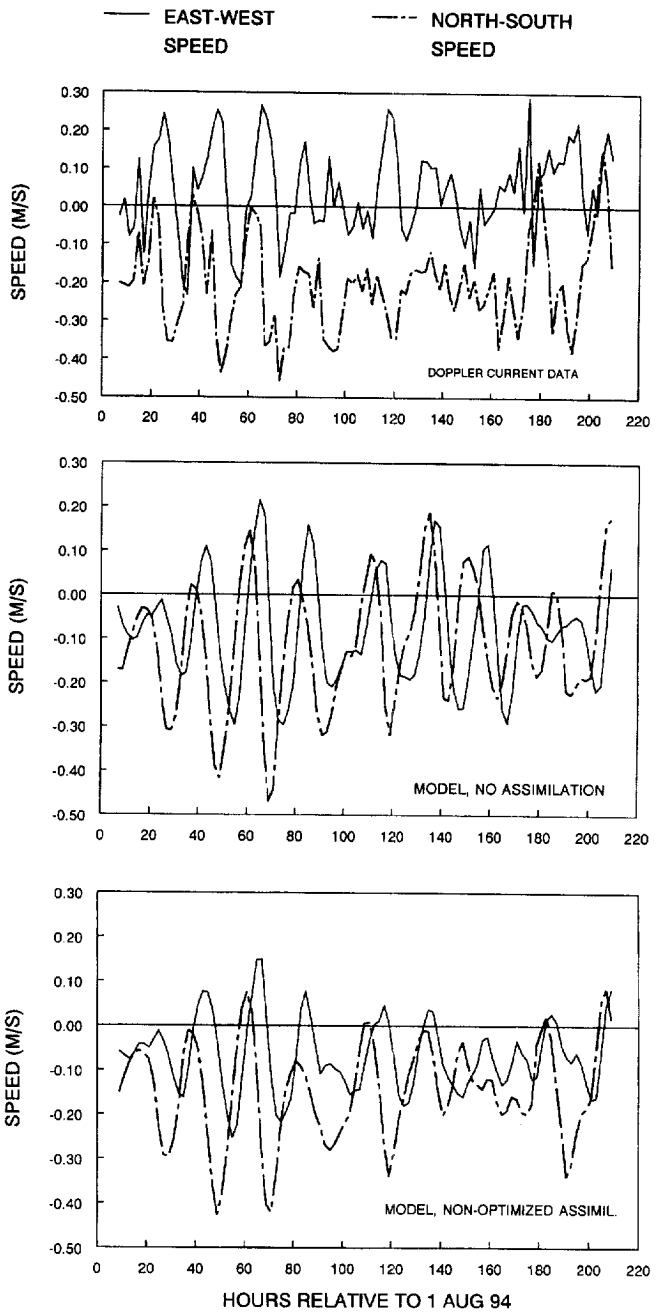

Fig. 3. Currents at station E (Fig. 1) as determined from a HF Doppler radar system (top), predicted by the model with no assimilation of Doppler current data (middle), and predicted by the model using a non-optimized assimilation technique (bottom). The model-predicted currents are for approximately the top 2 m of the water column.

movement of the water, with an average of ~ 20 cm/s. Paduan and Rosenfeld (1996) indicate that this southward flow is likely a result of the advection of wind-driven coastal upwelled water. The data are also seen to have higher frequency variations. Paduan and Rosenfeld (1996) showed that low-passed filtering the Doppler data resulted in better agreement with ADCP and drifter observations. This indicates that some of the higher frequency variations of the Doppler current data may be a result of measurement uncertainties of the HF radar system.

In some cases, the Doppler data covered a good portion of the model domain. But there were times during August 1994 in which the Doppler observations only covered a small portion of the domain (e.g., only the southern portion of the Monterey Bay itself). During instances in which there were data gaps at a particular grid cell, no assimilation was performed at that grid cell.

Wind velocity data were collected at a site at the mouth of Monterey Bay (Fig. 1). These wind data were applied to the entire model domain to provide an estimate of wind forcing during the simulation period. Variations of the magnitude of the calculated wind stress are shown in Fig. 4. We see a fairly regular cycle of enhanced wind stress at close to a diurnal cycle, with maximum stresses of about 1.5×10^{-4} Pa.

3.3. *Open boundary conditions*

The model uses results from the global tidal model of Schwiderski (1981, 1983) to specify the tidal surface height amplitudes and phases along the open boundaries of the ocean model. The model uses this sea level height information and the linearized equations of motion to specify the velocities along the open boundaries. Open boundary conditions of this type have at times been formulated without regard to the fact that longwave energy can be generated within the model domain (e.g., from wind forcing) and should be radiated out through the open boundaries. Such "clamped" boundary conditions can often lead to erroneous solutions (Lewis et al., 1994), and we wish to apply a condition that is better adapted for allowing longwave energy to leave the model domain.

For this study, we use an optimized approach for specifying the open boundary condition. Available information on the open boundary (the sea level heights from the global tide model) is combined with the physics of the model represented by the energy flux on the open boundary. The optimized open boundary condition is derived from the optimization problem

$$\min_{\eta}\left(J = 0.5g\int_S (gH)^{1/2}(\eta-\eta^{\circ})^2\,\mathrm{d}s\right),$$

$$-g\int_S H\eta u_n\,\mathrm{d}s = P_t,$$

where S is the open boundary, P_t the energy flux on the open boundary, u_n the vertically averaged outward normal velocity, η the model sea surface elevation on the open boundary, H the depth, g the acceleration due to gravity, and η° are the reference

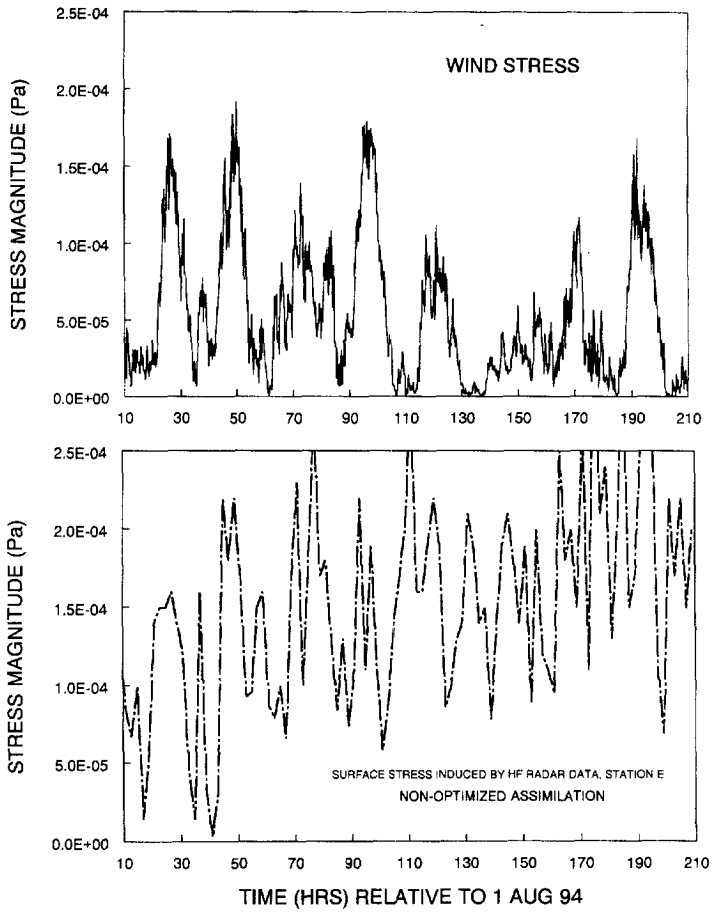

Fig. 4. Wind stress magnitude determined from observed wind velocity data near the mouth of Monterey Bay (top) and stress magnitude at Station E (Fig. 1) due to observed Doppler current data using a non-optimized assimilation technique (bottom).

values of the sea level elevation on the open boundary (i.e., the information from the global tide model). To solve the above, we use the regularization approach to obtain the following minimization problem:

$$\min_{\eta}\left[0.5\left(P_{\mathrm{t}}+g\int_S H\eta u_n\,\mathrm{d}s\right)^2+\gamma 0.5g\int_S (gH)^{1/2}(\eta-\eta^{\circ})^2\,\mathrm{d}s\right],$$

where γ is a parameter of regularization, chosen according to Shulman (1997) to provide the maximum of the entropy integral. The solution has the form

$$\eta=\eta^{\circ}+\lambda_t u_n(g/H)^{1/2},$$

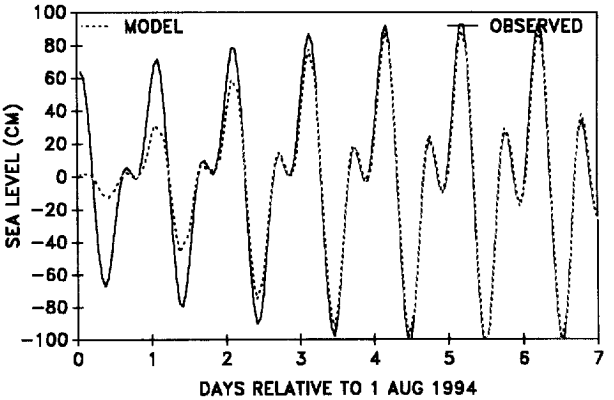

Fig. 5. Observed and model-predicted sea level variations for the six primary tidal constituents at a tide station located on the south side of Monterey Bay, California. The forcing of the model included the optimized open boundary condition formulation for tidal forcing as well as wind forcing (Fig. 4).

where

$$\lambda_t = -\left(P_t + g\int_S H\eta^\circ u_n \, ds\right)\Big/\left(g^{1/2}\int_S H^{3/2}u_n^2 \, ds + \gamma\right).$$

Thus, in the linearized momentum equations, the pressure gradient term due to horizontal sea level height variations uses $\eta^\circ + \lambda_t u_n(g/H)^{1/2}$ and the next model-predicted η in the interior of the model domain. In this way, any longwave radiation other than that generated directly by η° can be radiated out through the open boundary according to the $\lambda_t u_n(g/H)^{1/2}$ term.

The results of a test simulation using this optimization technique are shown in Fig. 5. The observed sea level variations at a site on the south side of Monterey Bay are reproduced by the model quite well, even with wind forcing.

4. Test simulations

For these simulations, model and Doppler currents were compared at the three locations indicated in Fig. 1 (west station W, central station C, and east station E). The model-predicted velocity corresponding to station E is shown in Fig. 3. This is from a model run without any assimilation of the HF Doppler current data in the model domain. Tidal variations are evident, and the variations are more smooth than the Doppler radar observations at the same location. The model predicts a southward and somewhat westward movement of the water, but the mean southward flow of $\sim$11 cm/s is only about half of that observed in the Doppler current data. The rms differences between the Doppler and model velocities for this particular location are 16.5 cm/s for the east-west component and 22.7 cm/s for the north–south component.

Table 2
Root mean square differences (cm/s) for a 210 h period during August 1994 between model-predicted and observed Doppler currents for the three stations shown in Fig. 1

	Station W		Station C		Station E	
	East–West	North–South	East–West	North–South	East–West	North–South
No assimilation of Doppler currents	20.1	27.2	14.2	17.9	16.5	22.7
Non-optimized assimil., $C_D = 10^{-3}$	16.8	19.9	12.1	15.3	12.7	17.7
Optimized assimil., $C_D = 10^{-3}$	16.9	19.4	12.0	14.9	12.0	17.4
Optimized assimil., $C_D = 10^{-2}$	12.8	13.1	8.9	9.6	6.9	10.5

Table 2 shows the rms differences for the other two stations, all of which are ~ 14 cm/s or greater.

We considered the magnitude of the stresses at the bottom of the model surface layer at the stations shown in Fig. 1. In general, the stress magnitudes and variations are quite similar to the wind stress (top graph in Fig. 4), indicating that much of the wind stress being applied to the surface layer of the model is being transferred through to the underlying level.

To quantify the degree to which the model currents reproduce the qualitative features of the Doppler currents, we calculated the linear and non-parametric rank correlations between the fields of Doppler velocities and the corresponding model-predicted surface velocities (Press et al., 1996). The time-varying correlations are shown in Fig. 6a for the linear correlation coefficient and Fig. 6b for the Spearman rank-order correlation coefficient. We see that at times there is a significant anticorrelation between model-predicted currents and the Doppler-observed currents. The mean correlations are approximately zero.

4.1. Non-optimized approach

Another simulation was performed assimilating all available Doppler radar velocities at the appropriate grid cells using Eq. (1). The value of C_D was set to 10^{-3}. The results at station E are shown in Fig. 3. The assimilation scheme has had an impact on the model predictions, reducing the rms differences between the Doppler radar and model velocities at station E to 12.7 cm/s for the east–west component and 17.7 cm/s for the north-south component. Similar reductions were seen at stations W and C (Table 2). In addition, there is now more of a southward drift to the flow field, with a mean of about 15 cm/s.

The additional stress at station E due to the HF Doppler current data is shown in Fig. 4. The magnitude of this shearing stress is relatively large, on average twice as great as the wind stress. It is also highly variable when compared to the variations of

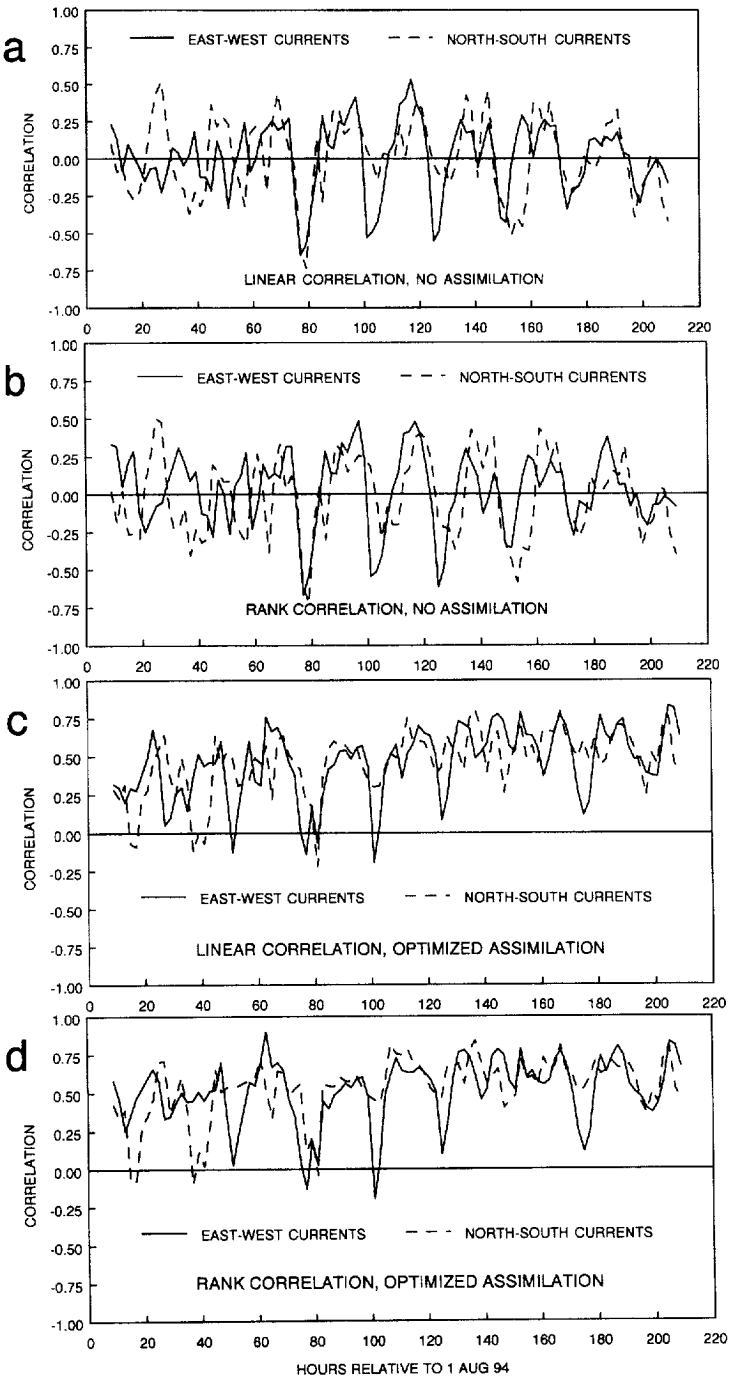
a
EAST-WEST CURRENTS
NORTH-SOUTH CURRENTS
CORRELATION
LINEAR CORRELATION, NO ASSIMILATION
b
EAST-WEST CURRENTS
NORTH-SOUTH CURRENTS
CORRELATION
RANK CORRELATION, NO ASSIMILATION
c
CORRELATION
EAST-WEST CURRENTS
NORTH-SOUTH CURRENTS
LINEAR CORRELATION, OPTIMIZED ASSIMILATION
d
CORRELATION
EAST-WEST CURRENTS
NORTH-SOUTH CURRENTS
RANK CORRELATION, OPTIMIZED ASSIMILATION
1.00
0.75
0.50
0.25
0.00
-0.25
-0.50
-0.75
-1.00
0
20
40
60
80
100
120
140
160
180
200
220
HOURS RELATIVE TO 1 AUG 94

the wind stress. This indicates that, for the non-optimized assimilation approach, the differences between the Doppler and model-predicted currents result in individual grid cells being subjected to relatively strong and variable shearing forces.

4.2. Optimized approach

Simulations were made using the optimized scheme represented by Eq. (2). The first simulation used $C_D = 10^{-3}$. The model-predicted velocity at station E is shown in Fig. 7. The rms differences at station E are nearly identical to those of the non-optimized assimilation results, 12.0 cm/s for the east-west component and 17.4 cm/s for the north–south component, with a mean southward flow of ~ 15 cm/s. However, the magnitude of the additional stress has been reduced considerably. Fig. 8 shows that the magnitude of the stress due to the differences between the observed and model-predicted currents at station E has been reduced dramatically, even to the point that the additional stress is typically less than the wind stress magnitude (top graph, Fig. 4). In terms of the linear and Spearman rank-order correlations, the assimilation of the Doppler current data increases the levels of correlation significantly (Fig. 6c and d). By the end of the simulation, the mean level of correlation is > 0.5.

A final simulation was made using the optimized scheme but with $C_D = 10^{-2}$. The increase of the drag coefficient provides a greater emphasis on driving the model toward the Doppler radar observations, and this is reflected in the results (Fig. 7 and Table 2). For this simulation, the rms differences at station E decreased to 6.9 cm/s for the east–west component and 10.5 cm/s for the north-south component. The model does a better job in reproducing the mean flows seen in the Doppler radar data (the predicted mean southward flow is now ~ 19 cm/s), but it is also beginning to pick up the higher frequency variability of the Doppler data. If we consider the drag at station E resulting from the HF Doppler data with $C_D = 10^{-2}$ (Fig. 8), we see that it has increased considerably, but it is still less than the drag for the non-optimized assimilation run.

5. Discussion

Doppler radar systems provide valuable information about surface currents, particularly the character of circulation patterns, trends, and relative magnitudes of currents. At the same time, the amplitudes and variations of Doppler radar currents can be very erroneous, with the magnitudes of errors at times the order of the currents.

Fig. 6. Results of correlation analyses between the HF Doppler surface current fields and the model-predicted surface current fields. (a) Linear correlation analysis between Doppler current fields and model results without assimilation of Doppler currents. (b) Rank correlation analysis between Doppler current fields and model results without assimilation of Doppler currents. (c) Linear correlation analysis between Doppler current fields and model results with optimized assimilation of Doppler currents ($C_D = 10^{-3}$). (d) Rank correlation analysis between Doppler current fields and model results with optimized assimilation of Doppler currents ($C_D = 10^{-3}$).

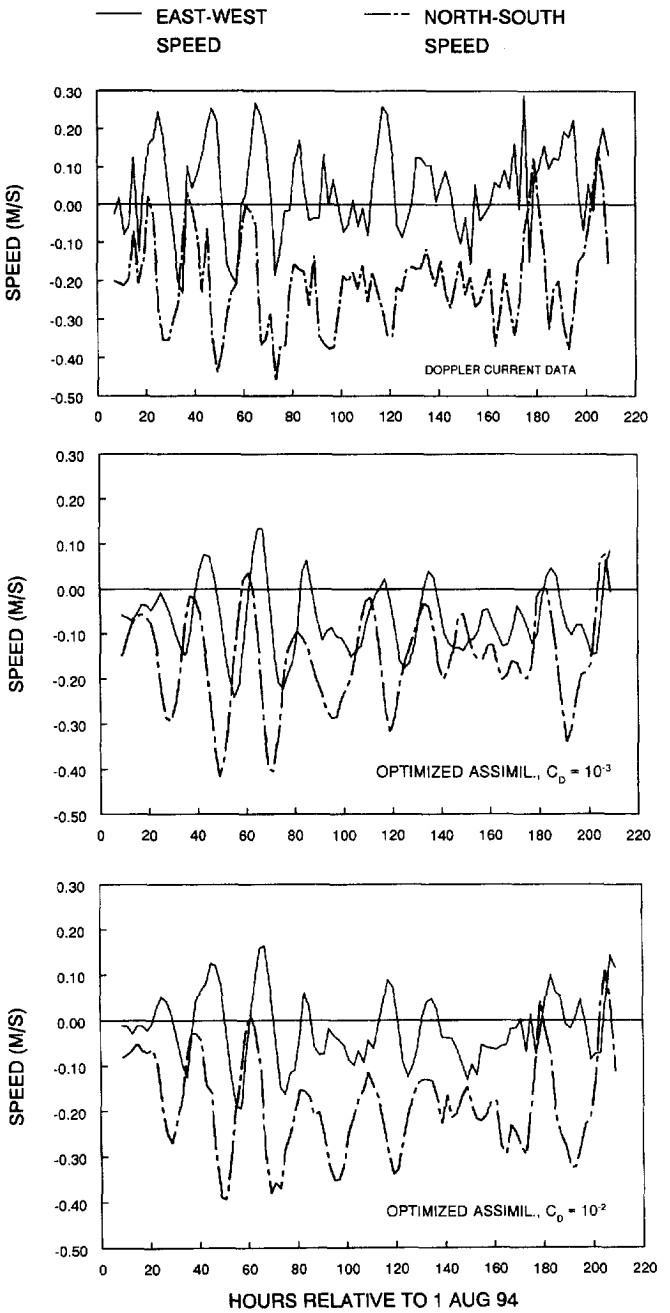

Fig. 7. Currents at station E (Fig. 1) as determined from a HF Doppler radar system (top), predicted by the model using the optimized assimilation technique with $C_D = 10^{-3}$ (middle), and predicted by the model using the optimized assimilation technique with $C_D = 10^{-2}$ (bottom). The model-predicted currents are for approximately the top 2 m of the water column.

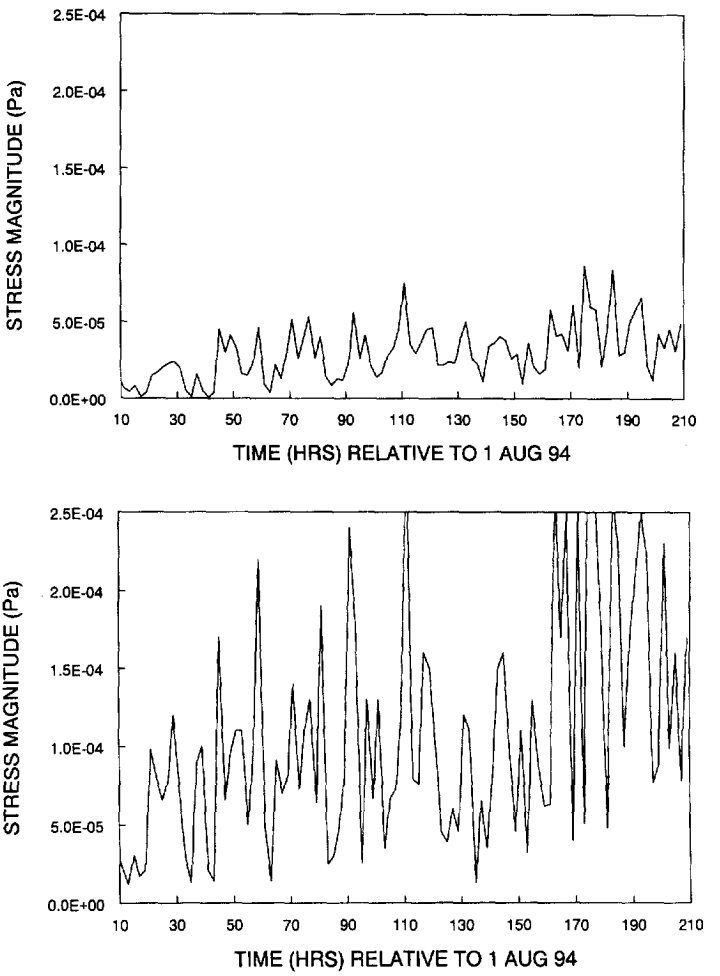

Fig. 8. Magnitude of the stress resulting from the differences between the Doppler and model-predicted currents at station E (Fig. 1). Doppler current data were assimilated using the optimized technique with $C_D = 10^{-3}$ (top) and $C_D = 10^{-2}$ (bottom).

Thus, care must be taken in the use of such observations due to the uncertainties in the accuracy of the data. Since we do not have reliable estimates of these errors, the assimilation of Doppler current data should be performed in the sense of the assimilation of qualitative characteristics such as current direction, trends, and circulation features.

We have proposed an approach for assimilating Doppler current data into ocean models based on the application of an additional shearing stress over the surface layer of the model. Since the stress results from the differences in model and Doppler current data, this approach can be interpreted as a special nudging technique in which the drag coefficient in the stress formulation plays the role of a nudging parameter. If

the differences between the model and observed currents are great enough at a particular grid cell, the resulting shearing stress can introduce a significant additional forcing in the model force balance equations. But when an optimization approach is employed, the additional stress has the minimal norm of all possible stresses performing the same work on the surface layer of the model.

The results of simulations with the Monterey Bay regional model show that the optimization approach results in a more gentle nudge of the model toward the Doppler currents when compared to a non-optimized assimilation technique. The results of the model with assimilation does a better job in reproducing some qualitative characteristics of the Doppler radar currents, as, for example, the prediction of a mean southward flow (station E, Fig. 7). The rms differences shown in Table 2 indicate that the optimized assimilation technique allows the model to reproduce the trends and variations of the Doppler current data with a much reduced stress level (Figs. 4 and 8). However, Table 2 also indicates that there are still some significant differences between the Doppler currents and the model surface currents. These differences are quite discernible when we look at the entire field of surface currents for a given time as shown in Fig. 9. The Doppler current field has a relatively strong and distinct circulation pattern when compared to the model simulation without any assimilation of the HF currents. The model-predicted surface currents with the Doppler current assimilation (also shown in Fig. 9) show that the assimilation has modified the currents to better match the pattern of the Doppler currents, but the match is far from perfect, and the magnitudes of the model-predicted velocities are small with respect to the Doppler velocities. This is even after more than 170 h of assimilating the fields of Doppler currents.

To further quantify the degree to which the assimilation scheme is forcing the model currents toward the qualitative features of the Doppler currents, we calculated the linear and non-parametric rank correlations between the fields of Doppler velocities and the model-predicted surface velocities. The correlations using model-predicted currents without any assimilation (Fig. 6a and b) have mean values of approximately zero. But with the assimilation of the Doppler current data, the mean correlation values increase significantly to > 0.5 (Fig. 6c and d). Thus, the assimilation technique is providing a practical means of ingesting the overall, qualitative characteristics of the Doppler current data (trends and patterns of circulation).

Although our results are encouraging, overall there is an indication of some problem with the model assimilating the Doppler current observations. Further investigation indicates that errors in the HF Doppler current data may be the primary reason that the model does not better respond to the continuous assimilation of the Doppler data. The physics incorporated into the ocean model conserves mass, and any breach of this conservation implied by the Doppler current data will be minimized by the model. For example, if the Doppler current data results in an unrealistic divergence/convergence in the surface layers of the ocean, the resulting pressure gradients in the model will generate currents opposite to those of the Doppler data. Thus, the overall ingestion of the Doppler currents will be reduced.

As a specific example, we calculated the divergence of two adjacent grid cells in the model based only on the HF Doppler currents. The results are shown in Fig. 10 and

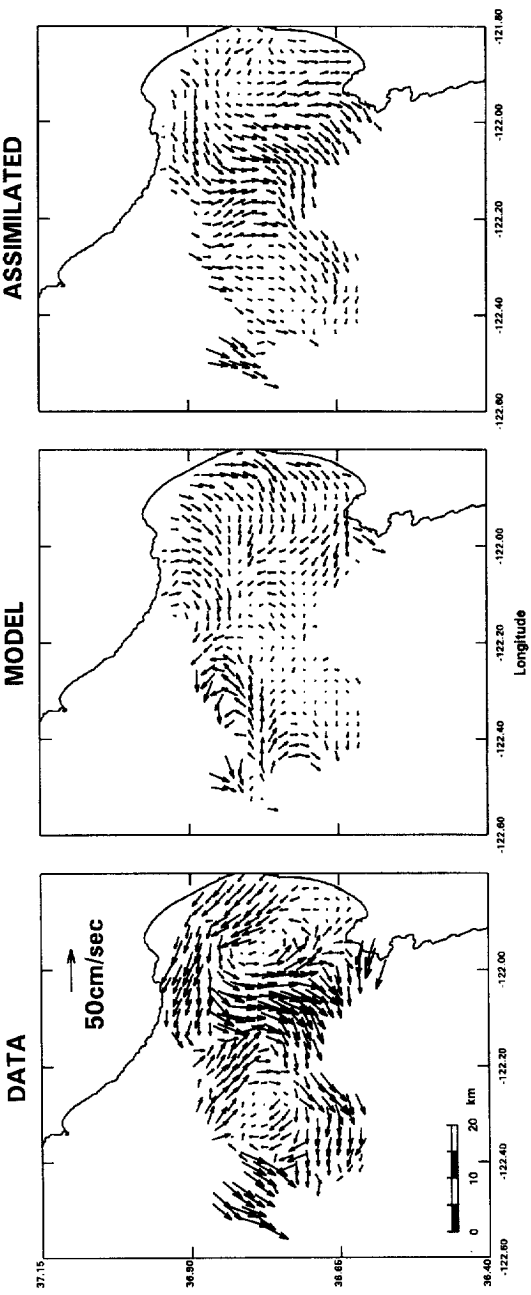

Fig. 9. Patterns of surface currents as determined by the HF Doppler currents (left), the numerical ocean model without any assimilation of the Doppler currents (middle), and the model with the optimized assimilation of the Doppler currents ($C_D = 10^{-3}$, right).

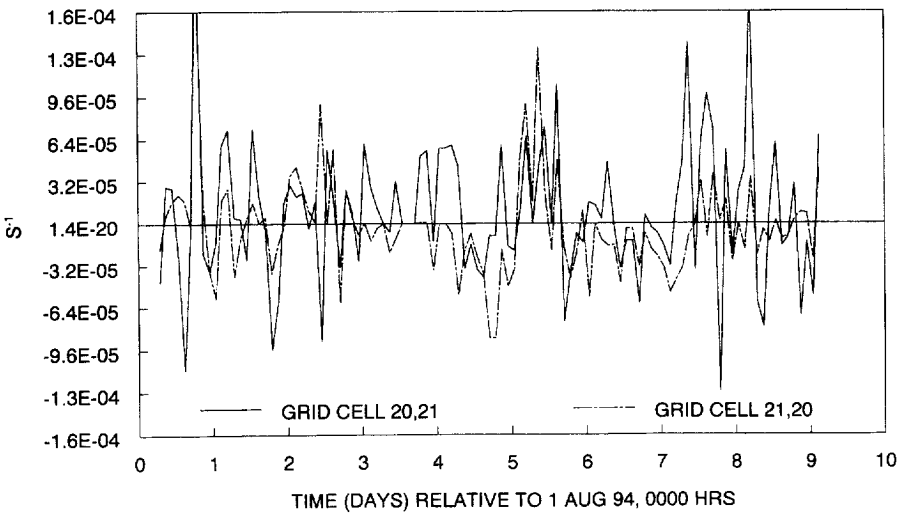

Fig. 10. Time histories of divergence based on the HF Doppler current data from two adjacent grid cells in the Monterey Bay regional ocean model.

indicate highly variable and large divergences and convergences. For the most part, we would not expect the magnitude of divergence in the ocean to be much larger than 10^{-6}/s. Yet the standard deviation of the variations of the Doppler-calculated divergence for these two grid cells is $\sim 4.5 \times 10^{-5}$/s, with maximum magnitudes reaching 1.6×10^{-4}/s. And there are a number of instances in which the divergences of the two grid cells are relatively large but opposite in sign. For a surface layer that was originally 2 m thick, the large but opposite-in-sign divergences over a two hour period would result in sea level differences between the two grid cells of the order of meters. This is over a distance of only about 2.8 km. The resulting pressure gradient in the model momentum equations would rapidly smooth out such a difference in sea level, minimizing the influence (assimilation) of the Doppler currents in the process.

These results suggest the additional processing of HF Doppler current data so as to further minimize errors in such data and to make the data more useful for various applications. Since the majority of observations and numerical studies show that surface currents have a divergence of the order of 10^{-6}/s, the output of HF Doppler radar systems could be smoothed, perhaps by fitting the field of currents with non-divergent (or near-non-divergent) eigenfunctions. This procedure has been performed using ocean drifter data by Eremeev et al. (1992a, b). In addition, Eremeev et al. (1992a) incorporated into their eigenfunctions the principle of no-flow perpendicular to a coastline (there are numerous examples of HF radar currents that show relatively strong, 20–30 min averaged currents flowing into or out of a shoreline). Such enhanced processing of HF Doppler current data could dramatically increase its accuracy and usefulness.

Acknowledgements

This work was supported by the Office of Naval Research, Naval Ocean Modeling Program, through a contract with HydroQual, Inc. The authors wish to thank Dr. J. Paduan for his help with the bathymetry and Doppler radar observations for the Monterey Bay region.

References

Blumberg, A.F., Mellor, G.L. 1987. A description of a three-dimensional coastal ocean circulation model. In: Heaps, N.S. (Ed.), Three Dimensional Coastal Models, Coastal and Estuarine Sciences, vol. 4, Amer. Geophys. Union Geophysical Monograph Board, 1–16.

Casulli, V., Cheng, R.T. 1992. Semi-implicit finite difference methods for three-dimensional shallow water flow. International Journal of Numerical Methods in Fluids 15, 629–648.

Eremeev, V.N., Ivanov, L.M., Kirwan, A.D., 1992a. Reconstruction of oceanic flow characteristics from quasi-Lagrangian data, 1: approach and mathematical methods. Journal of Geophysical Research 97, 9733–9741.

Eremeev, V.N, Ivanov, L.M., Kirwan, A.D., Margolina, T.M., 1992a. Reconstruction of oceanic flow characteristics from quasi-Lagrangian data, 1: characteristics of the large-scale circulation in the Black Sea. Journal of Geophysical Research 97, 9743–9753.

Lewis, J.K., Hsu, Y.L., Blumberg, A.F., 1994. Boundary forcing and a dual-mode calculation scheme for coastal tidal models using step-wise bathymetry. In: Spaulding, M., et al. (Eds.), Estuarine and Coastal Modeling III: Proceedings of the 3rd International Conference. Am. Soc. Civil Eng., pp. 422–431.

Mellor, G.L., Yamada, T., 1982. A hierarchy of turbulence closure models for planetary boundary layers. Journal of Atmospheric Science 31, 1791–1896.

Paduan, J.D., Rosenfeld, L.K. 1996. Remotely sensed surface currents in Monterey Bay from shore-based HF radar (Coastal Ocean Dynamics Application Radar). Journal of Geophysical Research 101 (C9), 20669–20686.

Press, W.H., Teukolsky, S.A., Vetterling, W.T., Flannery, B.P. 1996. Numerical Recipes in Fortran: The Art of Scientific Computing, Vol. 1. Cambridge Press, Cambridge.

Shulman, I. 1997. Local data assimilation in specification of open boundary conditions. Journal of Atmospheric and Ocean Technology 14, 1409–1419.

Smagorinsky, J. 1963. General circulation experiments with the primitive equations, I. The basic experiment. Monthly Weather Review 91, 99–164.

Schwiderski, E.W. 1981. Global ocean tides, Part V: the diurnal principal lunar tide O1, atlas of tidal charts and maps. Naval Surface Weapons Center, Silver Springs, MD. NSWC Technical Report 81–144, 15 pp.

Schwiderski, E.W. 1983. Atlas of ocean tidal charts and maps, Part I: the semidiurnal principal lunar tide M2. Marine Geodesy 6, 219–265.